Available online at www.sciencedirect.com
SCIENCE DIRECT®
ELSEVIER
International Journal of Heat and Mass Transfer 47 (2004) 2343–2352
International Journal of HEAT and MASS TRANSFER
www.elsevier.com/locate/ijhmt

An improved model of heat and moisture transfer with phase change and mobile condensates in fibrous insulation and comparison with experimental results

Jintu Fan [a,*], Xiaoyin Cheng [a], Xinhuo Wen [a], Weiwei Sun [b]

[a] *Institute of Textiles and Clothing, The Hong Kong Polytechnic University, Hung Hom, Kowloon, Hong Kong*
[b] *Department of Mathematics, City University of Hong Kong, Hong Kong*

Received 14 July 2002; received in revised form 29 October 2003

Abstract

This paper reports on an improved model of coupled heat and moisture transfer with phase change and mobile condensates in fibrous insulation. The new model considered the moisture movement induced by the pressure gradient, a super-saturation state in condensing region as well as the dynamic moisture absorption of fibrous materials and the movement of liquid condensates. The results of the new model were compared and found in good agreement with the experimental ones.

Keywords: Fibrous insulation; Phase change; Condensation; Moisture absorption; Heat and moisture transfer

1. Introduction

Theoretical modeling of coupled heat and moisture transfer with phase change in fibrous insulation started with Henry's work in 1930s [1]. However, little further progress has been made until 1980s. Ogniewicz and Tien [2] are the first workers who have contributed the subject through theoretical modeling and numerical analysis, assuming heat is transported by conduction and convection and the condensate is in pendulum state. The analysis was limited to a quasi-steady-state, viz. the temperature and vapor concentration remain unchanged with time before the condensates become mobile. Motakef and El-Masri [3] first considered the quasi-steady-state corresponding to mobile condensate, under which the condensates diffuse towards the wet zone's boundaries as liquid and re-evaporates at these boundaries leaving the time-invariant temperature, vapor concentration and liquid content profiles. This theoretical model was later extended by Shapiro and Motakef [4] to analyze the unsteady heat and moisture transport processes and compared the analytical results with experimental ones under some very limited circumstances. This analysis was only valid when the time scale for the motion of the dry–wet boundary in porous media is much larger than the thermal diffusion time scale, which may however not be the case with frosting and small moisture accumulation [5].

Farnworth [6] presented the first dynamic model of coupled heat and moisture transfer with sorption and condensation. This model was rather simplified and only appropriate for multi-layered clothing as it was assumed that the temperature and moisture content in each clothing layer were uniform. Vafai and Sarkar [7] first modeled the transient heat and moisture transfer with condensation rigorously. For the first time, the interface between the dry and wet zones was found directly from the solution of the transient governing equations. In this work, the effects of boundary conditions, the Peclet and Lewis number on the condensation process is numerically analyzed. Later Vafai and Tien [8] extended the analysis to two-dimensional heat and mass transport accounting for phase change in a porous matrix. Tao et al. [5] first analyzed the frosting effect in an insulation slab by

* Corresponding author. Tel.: +852-2766-6472; fax: +852-2773-1432.
E-mail address: tcfanjt@inet.polyu.edu.hk (J. Fan).

0017-9310/$ - see front matter © 2003 Elsevier Ltd. All rights reserved.
doi:10.1016/j.ijheatmasstransfer.2003.10.033

Nomenclature

C_a water vapor concentration in the inter-fiber void space ($kg\,m^{-3}$)
C_a^* saturated water vapor concentration in the inter-fiber void space ($kg\,m^{-3}$)
C_f water vapor concentration in the fiber ($kg\,m^{-3}$)
C_v effective volumetric heat capacity of the fibrous batting ($kJ\,m^{-3}\,K^{-1}$)
C_{vf} effective volumetric heat capacity of the fiber ($kJ\,m^{-3}\,K^{-1}$)
C_{va} volumetric heat capacity of the dry air ($kJ\,m^{-3}\,K^{-1}$)
C_{vv} volumetric heat capacity of water vapor ($kJ\,m^{-3}\,K^{-1}$)
C_{vw} volumetric heat capacity of water ($kJ\,m^{-3}\,K^{-1}$)
D_a diffusion coefficient of water vapor in the air ($m^2\,s^{-1}$)
D_f diffusion coefficient of moisture in the fiber ($m^2\,s^{-1}$)
D_l disperse coefficient of free water in the fibrous batting ($m^2\,s^{-1}$)
E the condensation or evaporation coefficient, dimensionless, $E = 5.0\text{E}{-3}$
ζ_i surface emissivity of the inner and outer covering fabrics ($i = 1$: inner fabric; $i = 2$: outer fabric)
F_R total thermal radiation incident traveling to the right ($W\,m^{-2}$)
F_L total thermal radiation incident traveling to the left ($W\,m^{-2}$)
h_c convective mass transfer coefficient ($m\,s^{-1}$)
h_t convective thermal transfer coefficient ($W\,m^{-2}\,K^{-1}$)
k effective thermal conductivity of the fibrous batting ($W\,m^{-1}\,K^{-1}$)
k_f thermal conductivity of fiber ($W\,m^{-1}\,K^{-1}$)
k_a thermal conductivity of air ($W\,m^{-1}\,K^{-1}$)
k_w thermal conductivity of water in the fibrous batting ($W\,m^{-1}\,K^{-1}$)
L thickness of the fabric batting (m)
M the molecular weight of the evaporating substance, $M = 18.0152$ (g/mol) for water
p partial water vapor pressure in the inter-fiber void (Pa)
p_a partial dry air pressure in the inter-fiber void (Pa)
p_t total air pressure in the inter-fiber void (Pa)
p_{sat} saturated water vapor pressure at temperature T_s (Pa)
P'_{sat} saturated vapor pressure at the temperature T_v (Pa)
p_v vapor pressure in vapor region at T_s (Pa)
u velocity of water vapor ($m\,s^{-1}$)
k_x permeability of porous batting (m^2)
μ dynamic viscosity of dry water vapor ($kg\,m^{-1}\,s^{-1}$)
r radius of fibers (m)
R the universal gas constant, $R = 8.314471 \times 10^7$ ($J\,K^{-1}\,mol^{-1}$)
r_i resistance to heat transfer of inner or outer covering fabric ($K\,m^2\,W^{-1}$) (i.e. $i = 0$: inner fabric, $i = L$: outer fabric)
RH_i relative humidity of the surroundings (%) (i.e. $i = 0$: surface next to human body, $i = L$: surrounding air)
Rhf relative humidity of the air space within the porous batting (%)
T_{bi} temperature of the boundaries (K) (i.e. $i = 0$: surface next to human body, $i = L$: surrounding air)
C_{ai} moisture concentration at the boundaries (K) (i.e. $i = 0$: surface next to human body, $i = L$: surrounding air)
T_s temperature at the interface of condensates and vapor (K)
T_v temperature in the vapor region (K)
t time (s)
w_i resistance to water vapor (i.e. $i = 0$: inner fabric, $i = L$: outer fabric) ($s\,m^{-1}$)
W_f water content of the fibers in the porous batting (%)
W water content of the fibrous batting (%)
W_c critical level of water content above which the liquid water becomes mobile (%)
W_i initial water content
W_{bi} weight of the ith layer of the batting before placing on the instrument in the cold chamber
W_{ai} weight of the ith layer of the batting before placing on the instrument in the cold chamber
WC_i water content of the ith layer of the batting
x distance from the inner covering fabric (m)

Greek symbols

ε porosity of the fibrous batting (ε = cubic volume of inter-fiber space/total cubic volume of batting space)
λ latent heat of (de)sorption of fibers or condensation of water vapor ($kJ\,kg^{-1}$)

ρ	density of the fibers ($\mathrm{kg\,m^{-3}}$)	β	radiative sorption constant of the fibers ($\mathrm{m^{-1}}$)
ρ_w	density of water ($\mathrm{kg\,m^{-3}}$)	σ	Boltzmann constant $\sigma = 5.6705 \times 10^{-8}$ ($\mathrm{W\,K^{-4}\,m^{-2}}$)
τ	effective tortuosity of the fibrous batting. The degree of bending or twist of the passage of moisture diffusion due to the bending or twist of fibers in the fibrous insulation. It normally changes between 1.0 and 1.2, depending on the fiber arrangements	Γ_s	the rate of (de)sorption ($\mathrm{kg\,s^{-1}\,m^{-3}}$)
		Γ_{ce}	the rate of condensation, freezing and/or evaporation ($\mathrm{kg\,s^{-1}\,m^{-3}}$)
		Γ	the total rate of (de)sorption, condensation, freezing and/or evaporation ($\mathrm{kg\,s^{-1}\,m^{-3}}$)

applying Vafai and Sarker's model to the case with temperature below the triple point of water. Tao et al. [9] have also for the first time considered the hygroscopic effects of insulation materials in the modeling. Murata [10] first considered the falling of condensate under gravity and built the phenomena into his steady-state model.

Fan et al. [11] first introduced dynamic moisture absorption process and radiative heat transfer as well as the movement of liquid condensates [12] in their transient models. The model [12] however was not examined by experiments. With the experimental results, the present work revealed that the previous model should be improved to consider the moisture bulk flow induced by the vapor pressure gradients. In this paper, the improved model is described and its results are compared with the experimental ones.

2. Model formulation

The model considers a clothing ensemble, consisting of a thick porous fibrous batting (~10 mm) sandwiched by one thin inner fabric (~0.1 mm) next to the human skin and the other layer of fabric (~0.1 mm) next to the cold environment. The schematic diagram is shown in Fig. 1. Since the fibrous batting is highly porous and the temperature difference between the human skin and the environment is great, radiative heat transfer within the fibrous batting is considered as important.

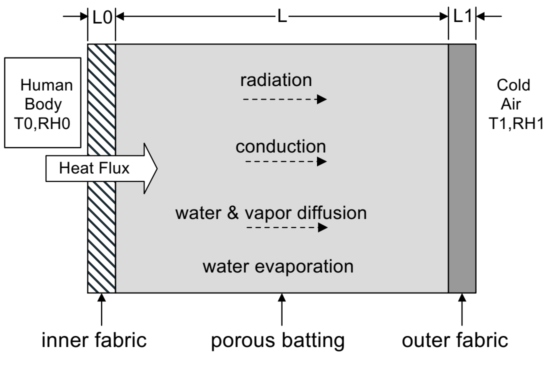

Fig. 1. Schematic diagram of the porous clothing ensemble.

In forming the mathematical model, we assume that

(1) The porous fibrous batting is isotropic in fiber arrangement and material properties.
(2) Volume changes of the fibers due to changing moisture and water content are neglected.
(3) Local thermal equilibrium exists among all phases and as a consequence, only sublimation is considered in the frozen region.
(4) The moisture content at the fiber surface is in sorptive equilibrium with that of the surrounding air.

The previous model reported by Fan and Wen [12] is the same as the new model except that the movement of moisture within the fibrous batting was neglected. This was found to be the cause of a large discrepancy between its numerical results and experimental ones. In the new model, it is believed that there is moisture movement within the batting induced by the pressure gradient—so called moisture bulk flow as in the case of wood drying [15]. The speed of the movement of moisture vapor (dry air is assumed as not moving as there is no dry air source from the skin on the left hand side) according to the Darcy's law is $u = -\frac{K_x}{\mu}\frac{\partial p_t}{\partial x}$, where $p_t = p_a + p$. Assuming the partial dry air pressure is unchanged, we have $\partial p_t/\partial x = \partial p/\partial x$, hence

$$u = -\frac{K_x}{\mu}\frac{\partial p}{\partial x} \tag{1}$$

where $p = p_{sat} \cdot Rhf$ is the partial pressure of water vapor in the inter-fiber void.

Based on the conservation of heat energy and applying the two-flux model of radiative heat transfer [11–13], at position x and time t, we have the heat transfer equation

$$C_v(x,t)\frac{\partial T}{\partial t} = -\varepsilon u C_{vv}(x,t)\frac{\partial T}{\partial x} + \frac{\partial}{\partial x}\left(k(x,t)\frac{\partial T}{\partial x}\right) + \frac{\partial F_R}{\partial x} - \frac{\partial F_L}{\partial x} + \lambda(x,t)\Gamma(x,t) \tag{2}$$

where the effective thermal conductivity $k(x,t)$ is a volumetric average calculated by $k(x,t) = \varepsilon k_a + (1-\varepsilon)(k_f + \frac{\rho}{\rho_w}Wk_w)/(1+\rho W/\rho_w)$, and the effective volumetric heat capacity of the fibrous batting is calculated by $C_v = \varepsilon C_{va} + \rho(1-\varepsilon)(C_{vf}\frac{\rho}{\rho_w}WC_{vw})/(1+\frac{\rho}{\rho_w}W)$. F_R is total thermal radiation incident at point x traveling to the right, i.e. from all angles in the left hand half space, and F_L is the total thermal radiation incident traveling to the left, i.e. from all angles in the right hand half space. Assuming that the angular distribution of radiative intensity is approximately constant so that F_R (from the hot side) is only slightly larger than F_L. This is justifiable since the temperature difference across a penetration depth (~1 K) is much less than the mean temperature of the sample (~300 K). With this assumption, the fraction of or that is absorbed by the fibers in the volume element can be characterized by an absorption constant β, which is an average over all angles of incidence and is independent of position. The absorptivity of the volume element is then $\beta\,dx$. The thermal emissivity of the volume element is also $\beta\,dx$ and equal power will be radiated into each half plane. We can therefore obtain the attenuation of the radiation fluxes as follows [13]:

$$\frac{\partial F_L}{\partial x} = \beta F_L - \beta\sigma T^4(x,t) \tag{3}$$

$$\frac{\partial F_R}{\partial x} = -\beta F_R + \beta\sigma T^4(x,t) \tag{4}$$

According to mass conservation, water vapor transfer in the inter-fiber void is controlled by the moisture transfer equation:

$$\varepsilon\frac{\partial C_a}{\partial t} = -\varepsilon u\frac{\partial C_a}{\partial x} + \frac{D_a\varepsilon}{\tau}\frac{\partial^2 C_a}{\partial x^2} - \Gamma(x,t) \tag{5}$$

Even when there is no condensation on the surface of a fiber in the porous batting (i.e. the relative humidity is less than 100%), fibers absorb or desorb moisture, the absorption or desorption rate is of the form:

$$\Gamma_s(x,t) = (1-\varepsilon)\frac{\partial C_f(x,t)}{\partial t} \tag{6}$$

where $C_f(x,t)$ is the moisture content within the fiber and obeys the Fickian diffusion [11].

When the relative humidity reaches 100%, condensation or freezing occurs in addition to absorption. Many previous models [3,5,9,12] assumed that extra moisture in the air is condensed instantaneously so that the maximum relative humidity in the air is 100%. This was considered as less appropriate and the cause of some discrepancies between the numerical results of the previous models and experimental results. It is now believed that there is a temporary super-saturation state or ($C_a > C_a^*$ or RH > 1.0), i.e. the moisture concentration in the air exceeding the saturated moisture concentration, time is required for the condensation to take place although, given sufficient time, the extra moisture in the air will condense until the moisture concentration in the air reduces to the saturated moisture concentration. On the other hand, when the humidity of surrounding air is below 100%, evaporation or sublimation occurs if there is free water or ice on the fiber surface.

Water condensation and evaporation are modeled using the Hertz–Knudsen equation [14]:

$$\Gamma_{ce}(x,t) = -E\sqrt{M/2\pi R}(P_{sat}/\sqrt{T_s} - P_v/\sqrt{T_v}) \tag{7}$$

From Eq. (7), we can get [12]

$$\Gamma_{ce}(x,t) = -E\sqrt{M/2\pi R}(1-\mathrm{RH})P_{sat}/\sqrt{T} \tag{8}$$

Therefore, the total water accumulation rate $\Gamma(x,t)$ is

$$\Gamma = \Gamma_s + \Gamma_{ce} \tag{9}$$

The free water, i.e. the water on the fiber surface, may diffuse when the free water is in liquid form and its content exceeds a critical value, according to the mass conservation, we have

$$\rho(1-\varepsilon)\frac{\partial \widetilde{W}}{\partial t} = \rho(1-\varepsilon)D_l\frac{\partial^2 \widetilde{W}}{\partial x^2} + \Gamma_{ce}(x,t) \tag{10}$$

where $\widetilde{W} = W(x,t) - W_f(x,t)$ is the free water content. $W_f(x,t) = C_f(x,t)/\rho$ is the water absorbed within the fiber; $W(x,t) = \frac{1}{\rho(1-\varepsilon)}\int_0^t \Gamma(x,t)\,dt$ is the total water content including that absorbed by the fibers and on the fiber surface.

D_l is defined phenomenologically, and depends on water content, temperature and properties of the fiber batting. $D_l = 0$ when the condensate is immobile, which is the case when the water content is less than a critical value W_c, or when the free water is frozen.

The boundary conditions to main differential equations (2) and (5) are the same as those reported previously [11,12]. Since the conductive heat transfer and moisture transport at the interfaces between the inner covering fabric and the batting as well as between the batting and the outer covering fabric should be continuous, we have

$$k_e\frac{\partial T}{\partial x}\bigg|_{x=0} = \frac{1}{r_0}(T|_{x=0} - T_{b0}) \tag{11}$$

$$k_e\frac{\partial T}{\partial x}\bigg|_{x=L} = \frac{T_{bL} - T|_{x=L}}{r_L + (1/h_t)} \tag{12}$$

$$\frac{D_a\varepsilon}{\tau}\frac{\partial C_a}{\partial x}\bigg|_{x=0} = \frac{1}{w_0}(C_a|_{x=0} - C_{a_{b0}}) \tag{13}$$

$$\frac{D_a\varepsilon}{\tau}\frac{\partial C_a^{n+1}}{\partial x}\bigg|_{x=L} = \frac{C_{a_{bL}} - C_a|_{x=L}}{w_L + (1/h_c)} \tag{14}$$

Considering the radiative heat transfer at the interface between the inner thin fabric and the fibrous batting and that between the outer thin fabric and the fibrous batting, we have initial conditions for Eqs. (3) and (4) as following

$$(1-\zeta_1)F_L(0,t) + \zeta_1\sigma T^4(0,t) = F_R(0,t) \tag{15}$$

$$(1-\zeta_2)F_{\mathrm{R}}(L,t)+\zeta_2\sigma T^4(L,t)=F_{\mathrm{L}}(L,t) \tag{16}$$

3. Numerical solution with finite difference scheme

We first consider the temperature $T(x,t)$ in the porous medium.

From Eqs. (3) and (4), we get

$$F_{\mathrm{L}}(x,t)=-\beta\sigma \mathrm{e}^{\beta x}\left[\int_0^x \mathrm{e}^{-\beta x}T^4(x,t)\,\mathrm{d}x+c_2\right] \tag{17}$$

$$F_{\mathrm{R}}(x,t)=\beta\sigma \mathrm{e}^{-\beta x}\left[\int_0^x \mathrm{e}^{\beta x}T^4(x,t)\,\mathrm{d}x+c_1\right] \tag{18}$$

Submit Eqs. (17) and (18) into Eqs. (3) and (4), we have

$$\frac{\partial F_{\mathrm{L}}}{\partial x}=-\beta^2\sigma \mathrm{e}^{\beta x}\left[\int_0^x \mathrm{e}^{-\beta x}T^4(x,t)\,\mathrm{d}x+c_2\right]-\beta\sigma T^4(x,t) \tag{19}$$

$$\frac{\partial F_{\mathrm{R}}}{\partial x}=-\beta^2\sigma \mathrm{e}^{-\beta x}\left[\int_0^x \mathrm{e}^{\beta x}T^4(x,t)\,\mathrm{d}x+c_1\right]+\beta\sigma T^4(x,t) \tag{20}$$

By using Eqs. (17) and (18) and the initial conditions (15) and (16), we obtain

$$c_1=\frac{\zeta_1}{\beta}T^4(0,t)-(1-\zeta_1)c_2 \tag{21}$$

$$\begin{aligned}c_2=&\frac{1}{(1-\xi_2)\beta(1-\zeta_1)\mathrm{e}^{-\beta L}-\beta \mathrm{e}^{\beta L}}\Bigg((1-\zeta_2)\\&\times\beta \mathrm{e}^{-\beta L}\int_0^L \mathrm{e}^{\beta k}T^4(k,t)\,\mathrm{d}k\\&+\beta \mathrm{e}^{\beta L}\int_0^L \mathrm{e}^{-\beta k}T^4(k,t)\,\mathrm{d}k+(1-\xi_2)\\&\times\zeta_1 \mathrm{e}^{-\beta L}T^4(0,t)+\zeta_2T^4(L,t)\Bigg)\end{aligned} \tag{22}$$

Submit (19) and (20) into (2), we obtain

$$C_{\mathrm{v}}(x,t)\frac{\partial T}{\partial t}=-\varepsilon u C_{\mathrm{vv}}(x,t)\frac{\partial T}{\partial x}+\frac{\partial}{\partial x}\left(k_e(x,t)\frac{\partial T}{\partial x}\right)+\Theta \tag{23}$$

where

$$\begin{aligned}\Theta=&\beta^2\sigma \mathrm{e}^{\beta x}\left[\int_0^x \mathrm{e}^{-\beta x}T^4(x,t)\,\mathrm{d}x+c_2\right]\\&-\beta^2\sigma \mathrm{e}^{-\beta x}\left[\int_0^x \mathrm{e}^{\beta x}T^4(x,t)\,\mathrm{d}x+c_1\right]\\&+2\beta\sigma T^4(x,t)+\lambda(x,t)\Gamma(x,t)\end{aligned} \tag{24}$$

Eq. (23) is a complex convection–diffusion equation. A finite difference scheme is applied to obtain the numerical solution. The time discretization scheme is semi-implicit Euler scheme, in which the linear convection term and diffusion term are implicit central finite difference scheme, and source term is explicit scheme. Since the source term Θ appears in nonlinear form, we used an explicit scheme for it, i.e. replacing it by the corresponding value at previous time step Θ_i^n. Consequently, at each time step, we only need to solve a linear tri-diagonal system. Accuracy of the scheme is first order in time, and second order in space.

A positive integer N is selected, and inscribed into the strip such that $\{(x,t): x\in[0,L], t\geqslant 0\}$. An irregular grid shown in Fig. 2 is chosen to get more precision in inflexions and save numeration time [17]. Denote by T_i^n the values of the temperature in x_i at time $n\Delta t$.

Using function derivatives in irregular grid (see Fig. 2), we have

$$\frac{\partial T}{\partial t}=\frac{T_i^{n+1}-T_i^n}{\Delta t} \tag{25}$$

$$\frac{\partial T}{\partial x}=\frac{T_{i+1}^{n+1}-T_{i-1}^{n+1}}{(s_E+s_w)\Delta x} \tag{26}$$

$$\begin{aligned}&\frac{\partial}{\partial x}\left(k(x,t)\frac{\partial T}{\partial x}\right)\\&=\frac{\left(k(x,t)\frac{\partial T}{\partial x}\right)\Big|_{x=x_i+\frac{1}{2}S_E\Delta x}-\left(k(x,t)\frac{\partial T}{\partial x}\right)\Big|_{x=x_i-\frac{1}{2}S_{\mathrm{w}}\Delta x}}{\left(\frac{(s_E+s_w)\Delta x}{2}\right)}\\&=\frac{k^n_{i+\frac{1}{2}S_E\Delta x}\frac{T_{i+1}^{n+1}-T_i^{n+1}}{s_E\Delta x}-k^n_{i-\frac{1}{2}S_{\mathrm{w}}\Delta x}\frac{T_i^{n+1}-T_{i-1}^{n+1}}{s_w\Delta x}}{\left(\frac{(s_E+s_w)\Delta x}{2}\right)}\\&=\frac{2}{(\Delta x)^2}\Bigg[\frac{k^n_{i+\frac{1}{2}S_E\Delta x}}{s_E(s_E+s_w)}T_{i+1}^{n+1}-\frac{1}{s_E+s_w}\Bigg(\frac{k^n_{i+\frac{1}{2}S_E\Delta x}}{s_E}\\&\quad+\frac{k^n_{i-\frac{1}{2}S_{\mathrm{w}}\Delta x}}{s_w}\Bigg)T_i^{n+1}+\frac{k^n_{i-\frac{1}{2}S_{\mathrm{w}}\Delta x}}{s_w(s_E+s_w)}T_{i-1}^{n+1}\Bigg]\end{aligned} \tag{27}$$

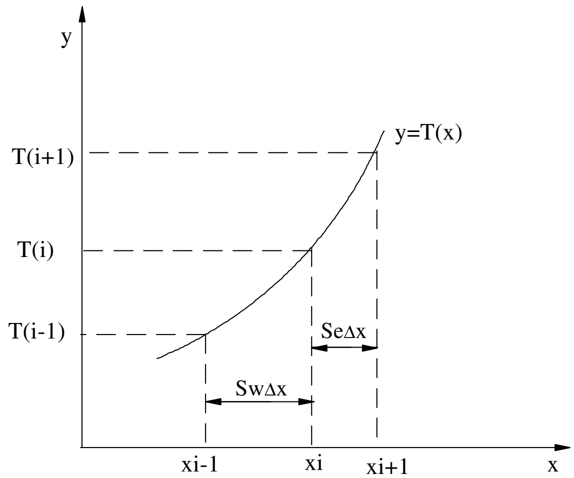

Fig. 2. Typical $T(x)$ showing function values T_{i-1}, T_i and T_{i+1} taken at unequally spaced base-points x_{i-1}, x_i and x_{i+1} where $x_{i+1}-x_i=s_E\Delta x$ and $x_i-x_{i-1}=s_w\Delta x$ $(0\leqslant s_E, s_w\leqslant 1)$.

Submit (25)–(27) into (23), we get the following finite difference scheme:

$$A_i^n T_{i-1}^{n+1} + B_i^n T_i^{n+1} + C_i^n T_{i+1}^{n+1} = D_i^n \quad (i = 1, 2, \ldots, N-1) \tag{28}$$

where

$$A_i^n = -\frac{\varepsilon_i^n u_i^n C_{\mathrm{vv}i}^n}{(s_E + s_w)\Delta x} - \frac{2}{(\Delta x)^2}\frac{k^n_{i-\frac{1}{2}s_w\Delta x}}{s_w(s_E + s_w)}$$

$$B_i^n = \frac{C_{\mathrm{v}i}^n}{\Delta t} + \frac{2}{(\Delta x)^2}\frac{1}{s_E + s_w}\left(\frac{k^n_{i+\frac{1}{2}s_E\Delta x}}{s_E} + \frac{k^n_{i-\frac{1}{2}s_w\Delta x}}{s_w}\right)$$

$$C_i^n = \frac{\varepsilon_i^n u_i^n C_{\mathrm{vv}i}^n}{(s_E + s_w)\Delta x} - \frac{2}{(\Delta x)^2}\frac{k^n_{i+\frac{1}{2}s_E\Delta x}}{s_E(s_E + s_w)}$$

$$D_i^n = \frac{C_{\mathrm{v}i}^n}{\Delta t} T_i^n + \Theta_i^n$$

Similarly, the finite difference scheme for moisture transfer in the inter-fiber voids is derived from Eq. (5):

$$\widetilde{A}_i^n C_{\mathrm{a}_{i-1}}^{n+1} + \widetilde{B}_i^n C_{\mathrm{a}_i}^{n+1} + \widetilde{C}_i^n C_{\mathrm{a}_{i+1}}^{n+1} = \widetilde{D}_i^n \quad (i = 1, 2, \ldots, N-1) \tag{29}$$

where

$$\widetilde{A}_i^n = -\frac{\varepsilon_i^n u_i^n}{(s_E + s_w)\Delta x} - \frac{2D_\mathrm{a}\varepsilon_i^n}{\tau(\Delta x)^2 s_w(s_E + s_w)}$$

$$\widetilde{B}_i^n = \frac{\varepsilon_i^n}{\Delta t} + \frac{2D_\mathrm{a}\varepsilon_i^n}{\tau(\Delta x)^2 s_E s_w}$$

$$\widetilde{C}_i^n = \frac{\varepsilon_i^n u_i^n}{(s_E + s_w)\Delta x} - \frac{2D_\mathrm{a}\varepsilon_i^n}{\tau(\Delta x)^2 s_E(s_E + s_w)}$$

$$\widetilde{D}_i^n = \frac{\varepsilon_i^n}{\Delta t} C_{\mathrm{a}i}^n - \Gamma_i^n$$

The finite difference scheme for free water diffusion is derived from Eq. (10):

$$\widehat{A}_i^n \widetilde{W}_{i-1}^{n+1} + \widehat{B}_i^n \widetilde{W}_i^{n+1} + \widehat{C}_i^n \widetilde{W}_{i+1}^{n+1} = \widehat{D}_i^n \quad (i = 1, 2, \ldots, N-1) \tag{30}$$

where

$$\widehat{A}_i^n = -\frac{2D_\mathrm{l}}{s_w(s_E + s_w)(\Delta x)^2}$$

$$\widehat{B}_i^n = \frac{1}{\Delta t} + \frac{2D_\mathrm{l}}{s_E s_w(\Delta x)^2}$$

$$\widehat{C}_i^n = -\frac{2D_\mathrm{l}}{s_E(s_E + s_w)(\Delta x)^2}$$

$$\widehat{D}_i^n = \frac{\widetilde{W}_i^n}{\Delta t} + \frac{\Gamma_{cei}^n}{\rho(1 - \varepsilon_i^n)}$$

The heat transfer equation (2), moisture transfer equation (5), and free water disperse equation (10) are coupled. In the computational procedure, we first solved the finite difference scheme for heat transfer (28) and got temperature $T(x,t)$. Secondly, we solved the finite difference scheme for moisture transfer (29) and got vapor concentration $C_\mathrm{a}(x,t)$. At each time step and each position, the computed vapor concentration $C_\mathrm{a}(x,t)$ was compared with the saturation vapor concentration $C_\mathrm{a}^*(T(x,t))$ at the corresponding temperature. If the calculated vapor concentration was greater than, or equal to, the saturation one (i.e. $Rhf \geqslant 1.0$), condensation takes place. Otherwise, evaporation or sublimation occurs. In the condensation region, if the temperature is above 0 °C, it is a wet region; if the temperature is below 0 °C, it is a freezing region. The condensation or evaporation rate was calculated by Eq. (9). At each time step and position, the calculated water content W was also compared with the critical water content W_c, under which no liquid water diffusion takes place. If $W > W_\mathrm{c}$, Eq. (29) was used to calculate the free water diffusion.

For the consideration of both stability and computational complexity, we chose a semi-implicit scheme. Usually, the scheme has much better stability than explicit scheme. The time step size $\Delta t = 0.1$ s and spatial step size $\Delta x = 0.1$ cm were adopted in simulation. For checking the convergence and stability of the scheme, we also computed with the time step size $\Delta t = 0.05$ and 0.01 s, and spatial step size $\Delta x = 0.05$ and 0.01 cm. The solutions obtained were almost the same, confirming the convergence and stability of the scheme.

4. Experiment

Experiments had been conducted using the instrument shown in Fig. 3. The device has a shallow water container 1 with a porous plate 3 at the top. The container is covered by a manmade skin 2 made of a waterproof, but moisture permeable breathable fabric. The edge of the breathable fabric is sealed with the container so that there is no water leakage. Water is supplied to the container from a water tank 16 through an insulated pipe 14. The water in the water tank is pre-heated to 33 °C. The water level at the water tank is checked frequently to ensure it is higher than the manmade skin so that water is in full contact with the manmade skin at the top of the container. The water temperature in the container 1 is controlled at 33 °C, simulating the human skin temperature. To prevent heat loss from the directions other than the upper right direction, the water container is surrounded with a guard with heating element 13. The temperature of the guard is controlled so that its difference from that of the bottom of the container is less than 0.2 °C. The whole device is further covered by thick insulation foam. The temperature

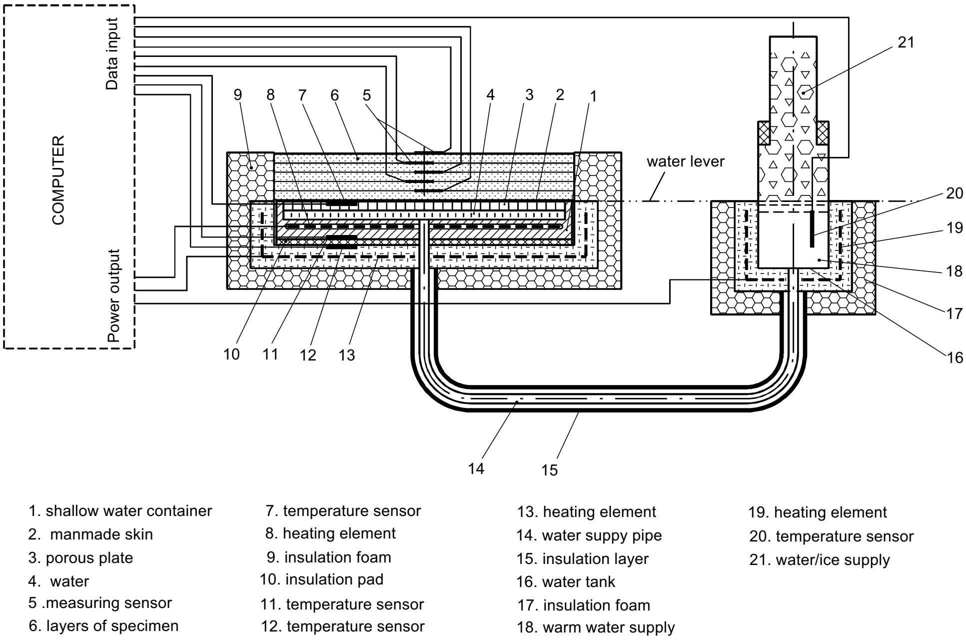

Fig. 3. Schematic design of the instrument.

measurement and control are achieved using a computer control system.

Multiple layers of two types of porous fibrous battings, one made of highly moisture absorbent viscose fibers and the other made of almost non-absorbent polyester fibers, sandwiched by a high density nylon lining fabric were tested on the above instrument in a cold chamber of -20 ± 1 °C and 90 ± 5 RH. The properties of the nylon lining fabric is listed in Table 1 and those of the two fibrous battings are listed in Table 2.

Ten plies of polyester battings making a total thickness of 4.92 cm and fifteen plies of viscose battings making the total thickness of 2.91 cm were tested, respectively. Each ply of the battings was conditioned in an air conditioned room of 20 ± 1 °C and 65 ± 5% RH and weighed using a electronic balance. The accuracy of the digital balance is 0.01 g. The net moisture weight of the batting is 0.1–4.0 g. The order of magnitude of the changes in the weights of the batting relative to the scale accuracy is 10–400. After placing the samples on the instrument in a cold chamber for a pre-determined time, each layer of the battings was re-weighed and the water content of the ith layer is then calculated by:

$$\mathrm{WC}_i = \frac{W_{ai} - W_{bi}}{W_{bi}} \times 100\% \tag{31}$$

Table 1
Properties of inner and outer covering fabric

Composition	Nylon
Weave	Woven
Mass (kg/m^2)	0.108
Thickness (m)	2.73E−04
Resistance to heat transfer $[r_0 = r_L]$ (K m^2 W^{-1})	3.15E−02
Resistance to water vapor transfer $[w_0 = w_L]$ (s m^{-1})	64.99
Resistance to air penetration (kPa s/m)	0.524
Coefficient of Darcy's law $[K_x/\mu]$ (m^2/(Pa s))	5.21E−07

Table 2
Properties of fibrous battings

Composition	Viscose	Polyester
Mass (kg/m^2)	0.145	0.051
Thickness of each layer (m)	1.94E−03	4.92E−03
Density of the fiber (kg/m^3)	1.53E+03	1.39E+03
Porosity	0.951	0.993
Resistance to air penetration (kPa s/m)	0.062	0.0061
Coefficients of Darcy's law (m^2/(Pa s))	3.106E−05	8.0607E−04

5. Numerical results and comparison with experimental ones

In the numerical computation, the initial condition is 20 °C and 65% RH. This is the condition under which the fibrous battings were conditioned before testing. In addition to the standard parameters which can be found from the handbooks, actually measured values of the parameters of fibrous battings and covering fabrics were used in the numerical computation except for the diffusion coefficient of moisture in the fiber D_f and the diffusion coefficient of free water on the fiber surface D_l. These two parameters were estimated through preliminary computational experiments so as to give best fit to the experimental results, as there are no experimental data available. $D_f = 1.512\text{E}{-16}$ m^2/s for viscose; $D_f = 1.0\text{E}{-16}$ m^2/s for polyester; $D_l = 5.4\text{E}{-11}$ m^2/s for viscose; $D_l = 1.35\text{E}{-13}$ m^2/s for polyester. For checking the sensitivity of model prediction to D_f and D_l, we computed with different D_f and D_l. The diffusion coefficient of moisture in the fiber D_f affects mainly the initial water content. The water content increases with the increase of D_f, but the general pattern of distribution is not changed with the change of D_f. The disperse coefficient of free water in the fibrous batting D_l affects the slope of water content distribution. When $D_l = 0.0$, there is no movement of liquid water on the fiber surface, the curve of water content distribution is concave, the peak appears at the outermost side of batting. With the increase of D_l, when the amount of liquid condensate exceeds a certain value, the liquid water overcomes the surface tension and moves to the region with a lower water content. When $D_l = 5.4 \times 10^{-8}$ m^2 s^{-1}, the distribution of water content is almost even. The critical water content (W_c) under which no liquid water diffusion takes place depends on the porosity and the surface tension of the fibers. Without accurate measurement, W_c was assumed to be 20% with reference to [16].

Figs. 4–7 compare the numerical and experimental results of water content distribution in fibrous battings.

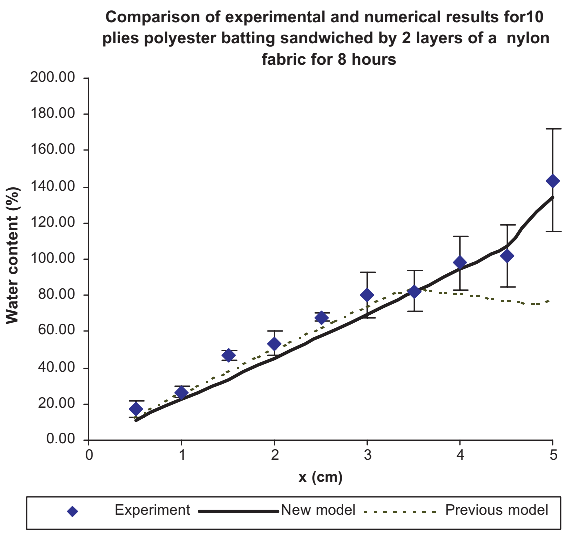

Fig. 4. Water content distribution for 8 h in battings (10 polyester layers + 2 nylon linings).

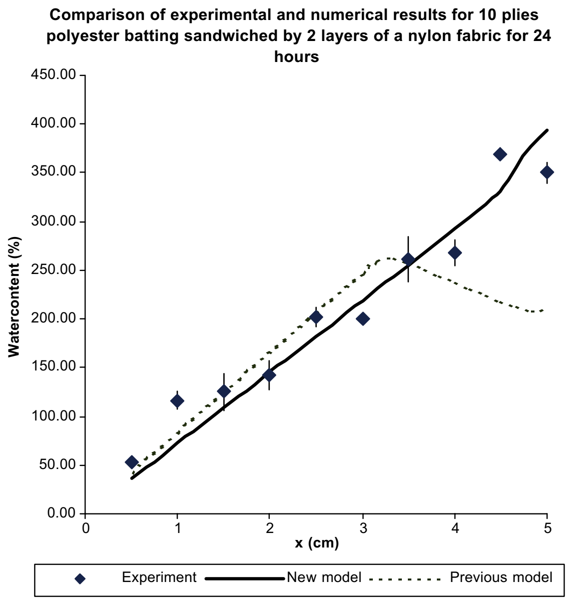

Fig. 5. Water content distribution for 24 h in battings (10 polyester layers + 2 nylon linings).

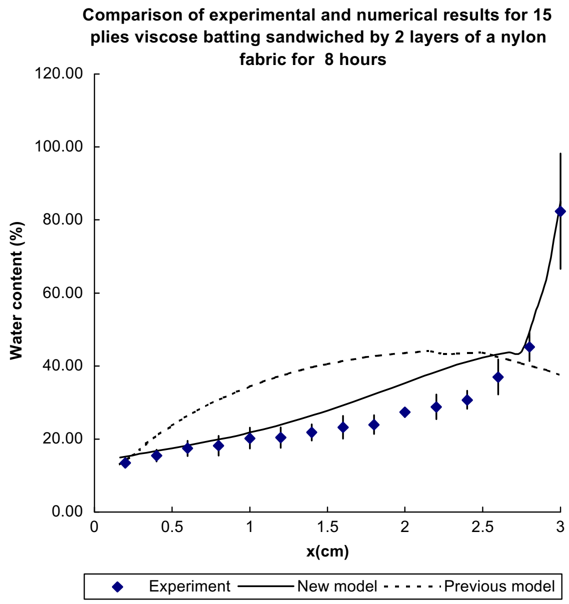

Fig. 6. Water content distribution for 8 h in battings (15 viscose layers + 2 nylon linings).

As can be seen, the numerical results of the new model fit well with the experimentally measured water content distribution in each of the four graphs, whereas those of the previous model [12] have large discrepancy from the experimental results in the outer (or colder) region of the fibrous battings. The largest relative error of the new

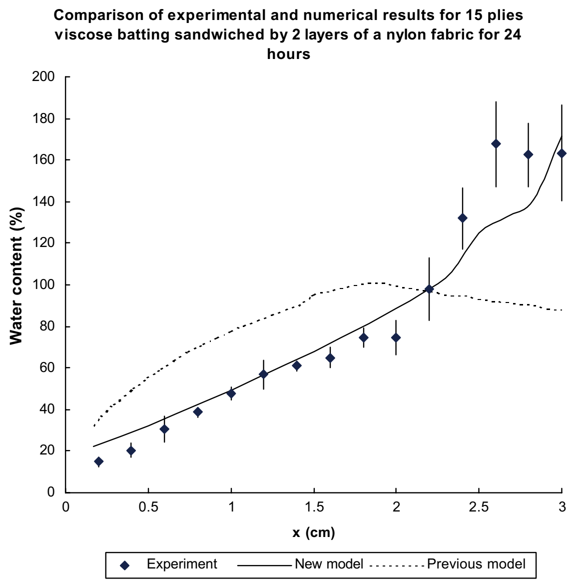

Fig. 7. Water content distribution for 24 h in battings (15 viscose layers + 2 nylon linings).

model prediction is 15%, whereas that of the old model prediction is 50%. Compared with the old model, the new model considered the moisture bulk flow and assumed to have a super-saturation state in the condensing region. It is believed that moisture bulk flow induced by the gradient of vapor pressure exists in the fibrous batting as the case in wood drying [15]. In addition to diffusion, moisture bulk flow transports moisture from the inner warmer region to the outer colder region. Increasingly more moisture is consequently accumulated in the outer region to form a super-saturation state, where high rate of condensation takes place. The condensation rate is the greatest at the interface between the outer layer of the batting and the outer covering fabric due to the much lower permeability of the outer covering fabric.

In most cases, the differences between the numerical results of the new model and the experimental ones are small (the error bars in the figures are one standard deviation). There are however some large differences at x from 1.2 to 2.8 cm in Fig. 6 (the largest relative error is 5%) and at x from 2.2 to 2.8 cm in Fig. 7 (the largest relative error is 15%). These differences may be due to the fact that we assumed constant values of model parameters, such as D_f, D_l and E, but in reality there are complex interactions between them as well as temperature, water content and humidity. Further modeling and experiments are needed to clarify these complex interactions.

From the experimental results plotted in Figs. 4 and 6, it can be noticed that there was a steep increase in the water content in the outermost layer of the batting in comparison with the second outermost layer of the batting after the ensembles were tested for 8 h in the cold chamber. However, the water contents between the outermost layer and the second outermost layer were not so much different when the ensembles were tested for 24 h in the cold chamber as shown in Figs. 5 and 7. This may be due to an experimental error in not accounting all the ice condensates at the interface between the outmost layer of the batting and the outer covering fabric as it was observed that, little ice was stick to the outer covering fabric after 8 h testing in the chamber, but a lot of ice was stick to the outer covering fabric after 24 h.

Figs. 8 and 9 compare the power supply in the experiments and the heat loss calculated through numerical computation. There is good agreement between the heat loss after stabilization calculated using

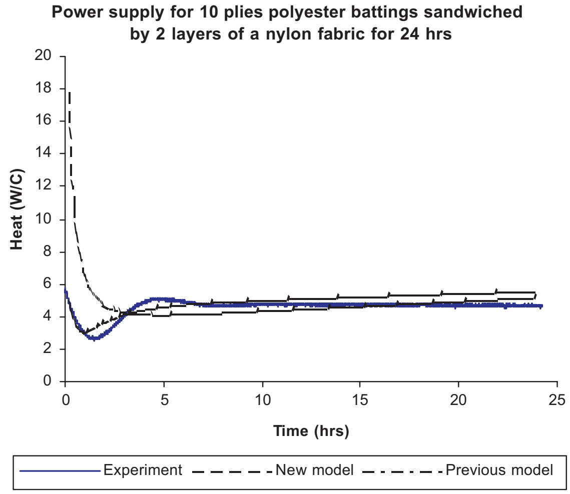

Fig. 8. Power supply for 10 plies polyester batting sandwiched by 2 layers of a nylon fabric.

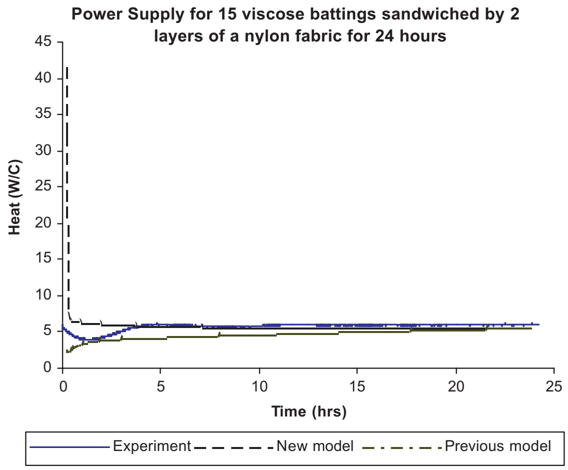

Fig. 9. Power supply for 15 plies viscose batting sandwiched by 2 layers of a nylon fabric.

our new model and power supply measured by experiments. The discrepancy occurred in the initial period of time is understandable. The new model predicted that heat loss reduces drastically in the initial half hour until reaching an almost stabilized value, whereas the experimental results showed that the power supply fluctuated for about 3–4 h until reaching an almost stabilized value. The calculated heat loss is reasonable as the clothing assembly is initially much warmer than the environment within the cold chamber (i.e. clothing assembly was placed into the cold chamber of −20 °C from the room temperature of 20 °C), causing high heat loss in the initial period of time. In the experiments, the high heat loss is however not simultaneously compensated by the heat supply of the experimental instrument. There is an inevitable time delay.

6. Conclusions

In this paper, we have presented an improved model of coupled heat and moisture transfer with phase change and mobile condensates in fibrous insulation. The new model considered the moisture movement within the batting induced by the pressure gradient, a super-saturation state in condensing region as well as the dynamic moisture absorption of fibrous materials and the movement of liquid condensates. The results of the new model were compared and found in good agreement with the experimental ones.

Acknowledgements

The authors would like to thank the Research Grant Committee of the Hong Kong University Grant Council for funding the project (PolyU 5142/00E). The work of W. Sun was supported in part by the City University of Hong Kong research grant 7001331.

References

[1] P.S.H. Henry, Diffusion of moisture and heat through textiles, Discuss. Faraday Soc. 3 (1948) 243–257.
[2] Y. Ogniewicz, C.L. Tien, Analysis of condensation in porous insulation, J. Heat Mass Transfer 24 (1981) 421–429.
[3] S. Motakef, M.A. El-Masri, Simultaneous heat and mass transfer with phase change in a porous slab, J. Heat Mass Transfer 29 (1986) 1503–1512.
[4] A.P. Shapiro, S. Motakef, Unsteady heat and mass transfer with phase change in porous slab: analytical solutions and experimental results, J. Heat Mass Transfer 33 (1990) 163–173.
[5] Y.X. Tao, R.W. Besant, K.S. Rezkallah, Unsteady heat and mass transfer with phase changes in an insulation slab: frosting effects, Int. J. Heat Mass Transfer 34 (1991) 1593–1603.
[6] B. Farnworth, A numerical model of the combined diffusion of heat and water vapor through clothing, Tex. Res. J. 56 (1986) 653–665.
[7] K. Vafai, S. Sarkar, Condensation effects in a fibrous insulation slab, J. Heat Transfer 108 (1986) 667–675.
[8] K. Vafai, H.C. Tien, A numerical investigation of phase change effects in porous materials, Int. J. Heat Mass Transfer 32 (1989) 1261–1277.
[9] Y.X. Tao, R.W. Besant, K.S. Rezkallah, The transient thermal response of a glass–fiber insulation slab with hygroscopic effects, Int. J. Heat Mass Transfer 35 (1992) 1155–1167.
[10] K. Murata, Heat and mass transfer with condensation in a fibrous insulation slab bounded on one side by a cold surface, Int. J. Heat Mass Transfer 38 (1995) 3253–3262.
[11] J. Fan, Z. Luo, Y. Li, Heat and moisture transfer with sorption and condensation in porous clothing assemblies and numerical simulation, Int. J. Heat Mass Transfer 43 (2000) 2989–3000.
[12] J. Fan, X. Wen, Modelling heat and moisture transfer, Int. J. Heat Mass Transfer 45 (2002) 4045–4055.
[13] B. Farnworth, Mechanics of heat flow through clothing insulation, Tex. Res. J. 53 (1983) 717–725.
[14] F.E. Jones, Evaporation of Water—with Emphasis on Application and Measurements, Lewis Publishers, MI, USA, 1992, pp. 25–43.
[15] Z. Chen, Primary Driving Force in Wood Vacuum Drying, Ph.D. Thesis, Virginia Polytechnic Institute and State University, 1997.
[16] J.L. Spencer-Smith, The physical basis of clothing comfort, Part 4: The passage of heat and water through damp clothing assemblies, Cloth. Res. J. 5 (1997) 116–128.
[17] D.R. Croft, D.G. Lilley, Heat Transfer Calculations Using Finite Difference Equations, Applied Science Publishers, London, England, 1977, pp. 47–50.